Materials Science & Engineering A 725 (2018) 228–241

Contents lists available at ScienceDirect

Materials Science & Engineering A

journal homepage: www.elsevier.com/locate/msea

Creep behavior and microstructural evolution of a 9%Cr steel with high B and low N contents

E. Tkachev*, A. Belyakov, R. Kaibyshev

Belgorod State University, Pobeda 85, Belgorod 308015, Russia

ARTICLE INFO

Keywords:
Martensite
Steel
Microstructure
Precipitation
Coarsening

ABSTRACT

The creep behavior of a 3%Co modified P92-type steel with high content of boron and low content of nitrogen was studied. The precipitation of Laves phase at lath boundaries provides a rapid decrease in the strain rate during transient creep. The finely dispersed (V,Nb)(C,N) carbonitrides uniformly distributed throughout and $M_{23}C_6$ carbides located at various boundaries/subboundaries result in extended steady-state creep. Gradual coarsening and an increase in the volume fraction of $M_{23}C_6$ carbides as well as coarsening of Laves phase particles is accompanied by an increase in the lath size during the steady-state creep. The coarsening of lath structure that is assisted by the dissolution of Laves phase particles at lath boundaries during steady-state creep leads to the onset of tertiary creep with a highly accelerated rate. The well-developed subgrain structure is observed in the ruptured samples, whereas the distance between high-angle boundaries does not change during the creep.

1. Introduction

High-chromium martensitic steels are widely used as creep resistant structural materials for various fossil power plant elements, which are exploited at elevated temperatures [1,2]. A P92-type steel alloyed with 0.1%C, 9%Cr, 2%W, 0.5%Mo, 0.2%V, 0.05%Nb is a typical representative of such steels [1–5]. Their alloying composition is designed to provide a long-term creep resistance at high temperatures. Normalizing at 1323 K followed by tempering at approx. 1023 K produces the tempered martensite lath structure (TMLS), which is composed of prior austenite grains (PAGs), packets, blocks, and laths with a high dislocation density [1,2,4,6]. The strengthening mechanisms include solid solution strengthening, dispersion strengthening, dislocation strengthening, etc. The solid solution strengthening is provided by such interstitial solutes as carbon and nitrogen and substitutional solutes of W, Mo and Cr. The dispersion strengthening is provided by numerous nanoscale (V,Nb)(C,N) carbonitrides precipitated in ferrite matrix [1–4] and $M_{23}C_6$ carbides located at any boundaries/subboundaries [7–9]. The long-range internal elastic stress fields originated from lath boundaries and lattice dislocations also contribute to superior creep resistance of these steels [6–10].

A degradation of TMLS under creep reduces the creep strength and leads to the creep strength breakdown that strongly diminishes the long-term creep strength [11–17]. The finely dispersed carbonitrides and boundary carbides play a key role in stability of TMLS under creep condition [1–4,8–14]. The $M_{23}C_6$ carbides located at lath boundaries exert a high Zener drag force and play a major role in the stability of TMLS under creep conditions [4,11–14]. The Laves phase particles precipitated during creep at low- and high-angle boundaries may also contribute to the TMLS stability [4,11–14]. The Zener drag force associated with (V,Nb)(C,N) carbonitrides is relatively low [4,11–14]. However, these dispersoids slows down the knitting reaction between the dislocations and lath boundaries. This reaction leads to transformation of the lath boundaries, which are irregular dislocation networks exhibiting long-range stress fields, into sub-boundaries, thereby relieving the internal stress fields [8,14,18].

The following changes among the dispersed particles may occur during long-term aging and creep [4,11–14,19,20]: (i) precipitation of Laves phase that leads to depletion of W and Mo from ferritic matrix down to thermodynamically equilibrium values; (ii) coarsening of $M_{23}C_6$ carbides, Laves phase particles, and (V,Nb)(C,N) carbonitrides; (iii) replacement of nanoscale V-rich (V,Nb)(C,N) carbonitrides by coarse particles of Z-phase through (V,Nb)(C,N)→Cr(V,Nb)N transformation. Such changes in distribution of secondary phase particles decrease the efficiency of solid solution strengthening and dispersion strengthening. In addition, these processes facilitate the knitting reactions leading to transformation of TMLS into subgrain structure, and thus diminish the dislocation strengthening. As a result, the high Cr steels gradually loose creep resistance under long-term creep conditions [21].

* Corresponding author.
E-mail address: tkachev_e@bsu.edu.ru (E. Tkachev).

https://doi.org/10.1016/j.msea.2018.04.032
Received 20 February 2018; Received in revised form 6 April 2018; Accepted 7 April 2018
Available online 10 April 2018

Table 1
Chemical composition of the modified P92 steel (wt%).

C	Si	Mn	Cr	W	Mo	Nb	V	Co	Ni	Cu	Ti	Al	N	B	Fe
0.1	0.12	0.4	9	1.5	0.57	0.05	0.2	2.8	0.24	0.027	0.002	0.01	0.007	0.012	Bal.

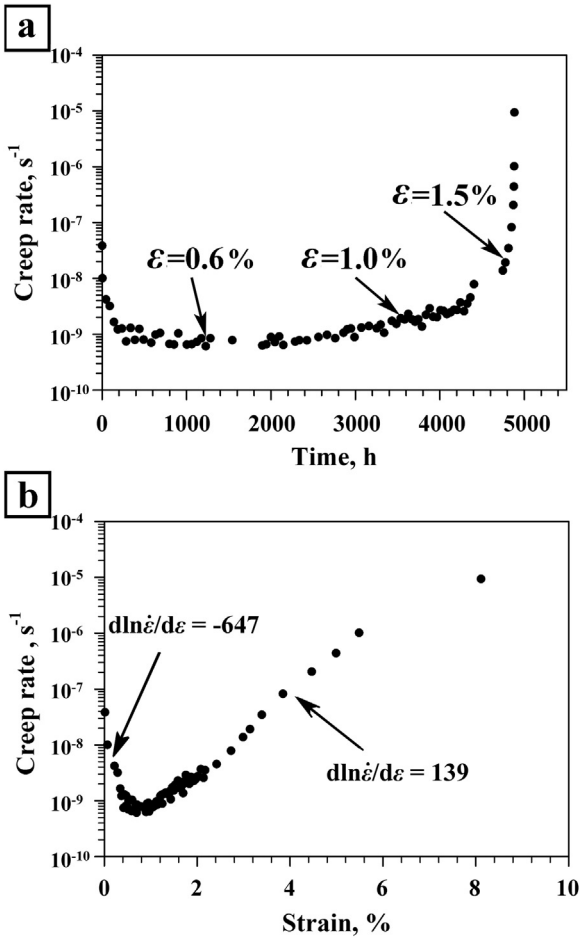

Fig. 1. Creep rate versus creep time (a) and creep rate versus strain (b) curves for the modified P92 steel subjected to creep tests at 923 K under 118 MPa. Arrows on creep rate versus creep time curve indicate the creep times at which the creep tests were interrupted.

The coarsening rate of Laves phase particles is the highest among the dispersed particles mentioned above, while the coarsening of (V,Nb)(C,N) carbonitrides occurs with the lowest rate [22,23]. The two-phase separation of carbonitrides to V-rich (V,Nb)(C,N) enriched by N and Nb-rich (V,Nb)(C,N) enriched by C plays an important role in the coarsening resistance [1,2,11–14]. The two-phase separation is provided by a special chemical composition of 0.1C-0.05N-0.024–0.07Nb (wt%) [1,2]. Regarding the $M_{23}C_6$ carbides, their coarsening rate could be decreased significantly by increasing boron content [23]. The high boron content provides the formation of B-free $M_{23}C_6$ carbide and $M_{23}(B,C)_6$ phase [23–25]. The $M_{23}(B,C)_6$ phase is much more resistant to coarsening than the B-free $M_{23}C_6$ carbides because of decreased energy of the $Fe_\alpha\{110\}||M_{23}(C,B)_6\{111\}$ interfaces [14,24]. The steels with high boron content have a low nitrogen content to prevent the formation of BN playing a role of embrittlement agent [1,14,26]. As a result, these steels contain a dispersion of (V,Nb)(C,N) carbides with increased portion of Nb-rich particles enriched by C [25,27]. The high Cr steels with high B and low N contents exhibits superior long-term creep [1,14,27,28], although, the structural mechanisms responsible for the creep strength improvement are still unclear. The aim of the present paper is to clarify the evolution of TMLS and dispersed particles in a modified P92-type steel with 3%Co, 0.012%B, and 0.007%N during creep at 923 K in comparison with conventional P92 and P92 + 3%Co steels.

2. Experimental

The chemical composition of the studied steel is presented in Table 1. The steel is characterized by a relatively large content of boron (0.012%), while the nitrogen content is reduced (0.007%) to avoid the formation of boron nitride (BN) and to suppress the formation of undesirable Z-phase during creep. The steel was produced by vacuum induction melting and then subjected to solution treatment at 1423 K followed by hot forging. Then, the steel was austenized at 1333 K for 0.5 h, air cooled, and tempered at 1023 K for 3 h. The creep specimens of 7 × 3 mm^2 in cross section and 25 mm in gauge length were subjected to tensile creep tests under 118 MPa at 923 K using ATS2330 lever arm machines. The hardness in the grip and gauge portions of crept specimens was measured using Brinell tests with a load of 750 N and a ball diameter of 5 mm.

The microstructural changes were studied using an FEI Nova NanoSEM 250 scanning electron microscope (SEM) incorporating an electron backscatter diffraction (EBSD) analysis. The dislocation substructures and finely dispersed precipitations were investigated by transmission electron microscopy (TEM) of thin foils and extracted carbon replicas using a Jeol JEM-2100 equipped with an INCA energy-dispersive X-ray spectrometer (EDS). The TEM foils were prepared by the double jet electro-polishing method using a 10% solution of perchloric acid in glacial acetic acid, applying a voltage of 20.5 V at room temperature. The transverse lath/subgrain sizes were measured on the TEM micrographs by a linear intercept method, counting all clear defined high-angle boundaries and low-angle subboundaries. The dislocation densities were estimated by counting the individual dislocations in the lath/subgrain interiors on at least ten arbitrarily selected typical TEM images. More than 100 particles of each precipitate type were quantified for each sample using extraction replicas. The mean particle size was calculated as $D = (a+b)/2$, where a and b are the short and long intercepts, respectively. The precipitates were identified by both the chemical analysis (EDS) and the selected area diffraction (SAD) method. The number of particles per unit area (N_S) was measured by counting the individual particles on the extraction carbon replicas. The volume fractions of precipitates were estimated using the following equation:

$$F_v = (2/3)\cdot N_S\cdot\pi\cdot r^2 \quad (1)$$

where r is the radius of particles. The equilibrium phase volume fractions and chemical compositions were calculated with ThermoCalc database TCFE7.

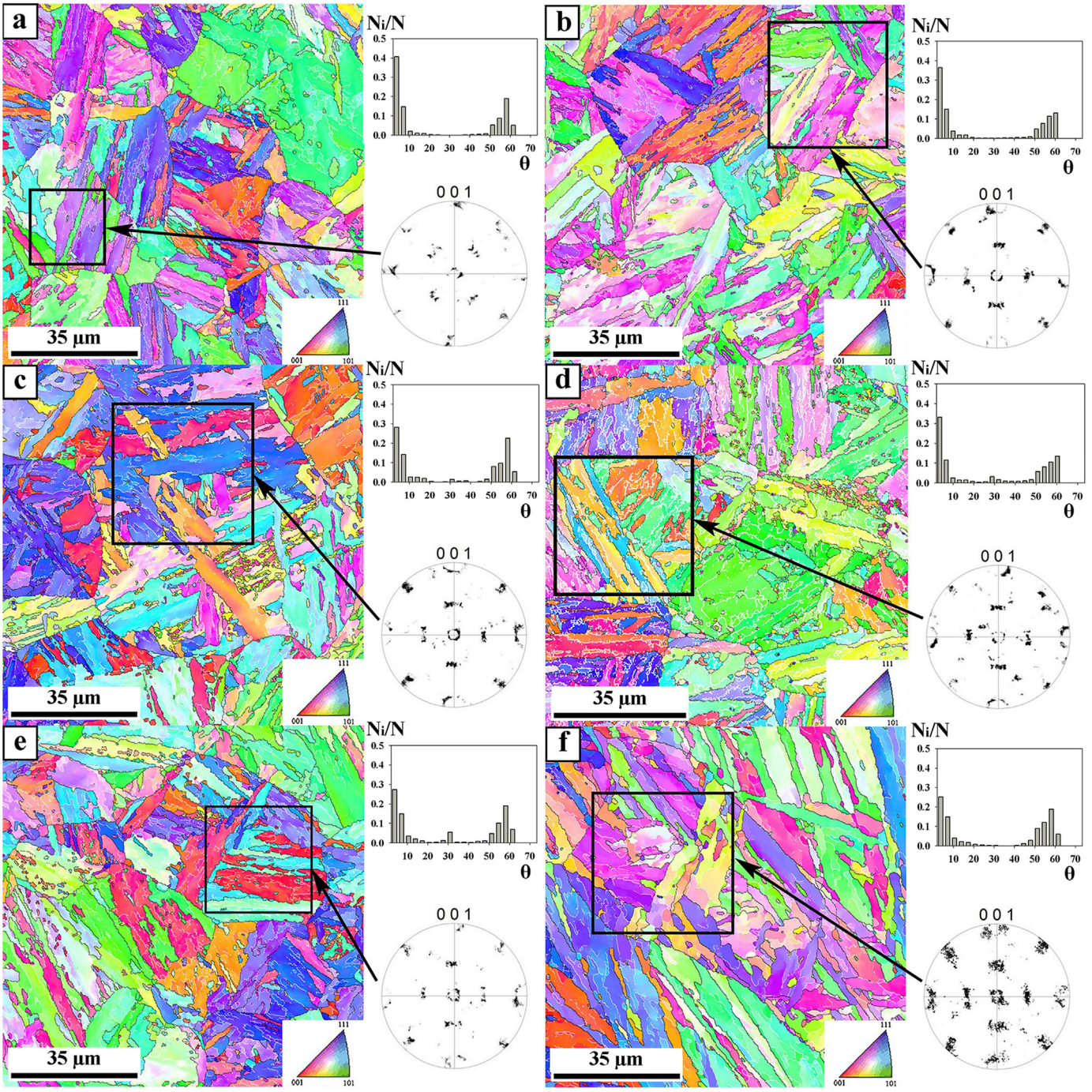

Fig. 2. Orientation maps for microstructures evolved in the modified P92 steel (N/N_i is the boundary fraction and θ is the misorientation angle): as-tempered (a); after long-term aging for 4701 h (b); after creep tests for 1031 h (c); 3532 h (d); 4701 h (e); 4883 h (f).

3. Results

3.1. Creep behavior

The creep rate versus time/strain curves are shown in Fig. 1. The present steel is characterized by an improved creep resistance. The time to rupture was 4883 h, which is more than 2.5 times longer than that in other P92-type steels under the same creep conditions [4,5,8,29]. Three distinctive creep stages, i.e. transient creep, steady-state creep, and accelerated creep, can be clearly recognized in Fig. 1. Transient creep leads to a decrease in the creep rate by a factor of 100 down to 10^{-9} s^{-1}. The onset of steady-state flow takes place at a creep strain of about 0.5% after 300 h. The steady-state creep takes place during 4200 h up to a strain of $\varepsilon \sim 1.2\%$. Then, the creep rate rapidly increases followed by a failure after 4883 h at total strain of $\varepsilon \sim 7\%$. The microstructural changes during creep were examined using interrupted creep tests

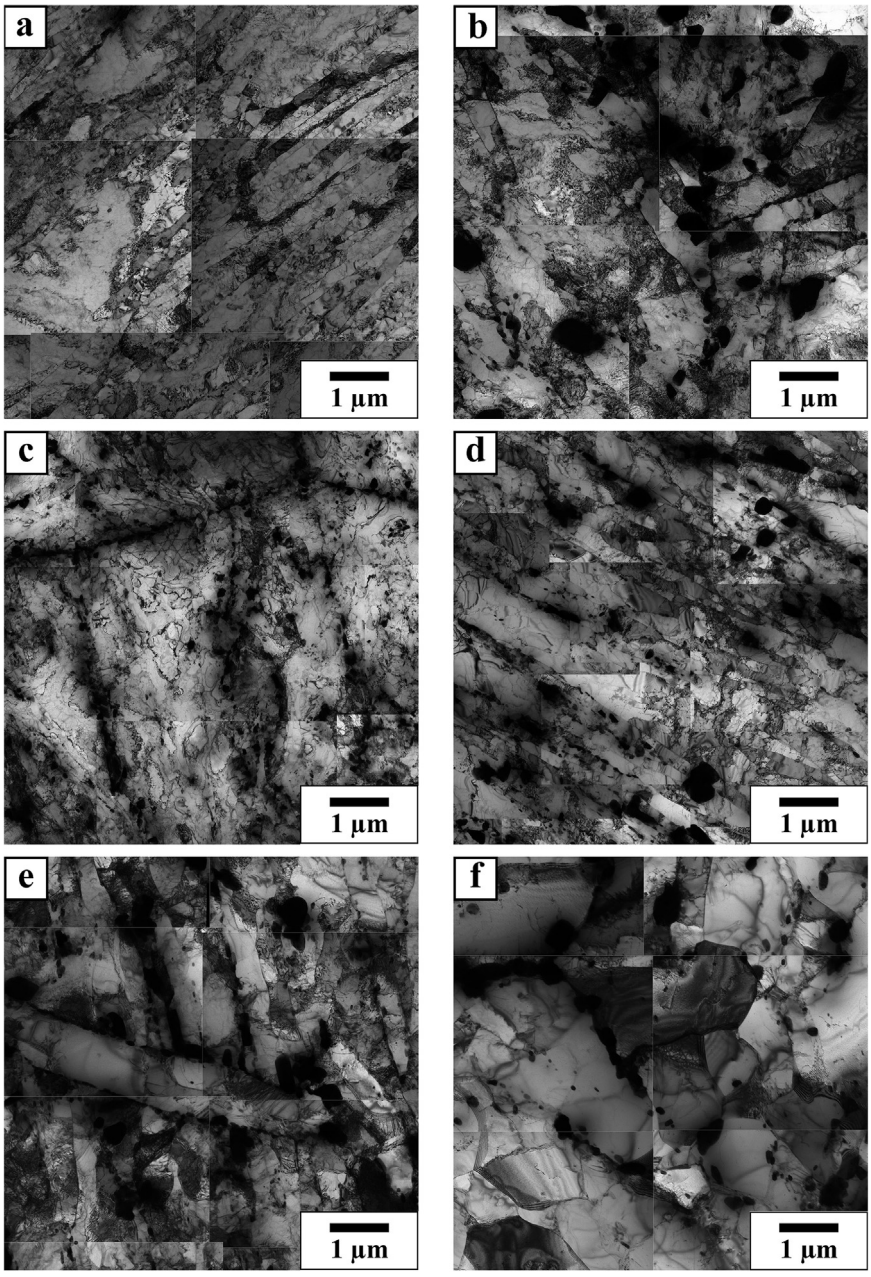

Fig. 3. Microstructures of the modified P92 steel (TEM): as-tempered (a); after long-term aging for 4701 h (b); after creep tests for 1031 h (c); 3532 h (d); 4701 h (e); 4883 h (f).

[4,18], when the creep test was stopped at strains of 0.6% (crept for 1031 h), 1.0% (crept for 3532 h), and 1.5% (crept for 4701 h), corresponding to the beginning of steady-state creep, approaching the end of steady-state creep, and tertiary creep, respectively, as indicated in Fig. 1a.

The creep rate versus strain curve of the present steel differs from those of other high Cr steels by significantly higher absolute values of $d\ln\dot{\varepsilon}/d\varepsilon$ for the transient and tertiary stages in Fig. 1b [14,30,31]. Therefore, the rearrangement of dislocations into a stable configuration through the first-order reaction-rate kinetics [14,30,32] in the present steel occurs at transient creep with the highest rate among all high Cr steels, for which these data are available. Concurrently, the present steel exhibits the significantly faster kinetic of the creep strength degradation at tertiary creep stage in comparison with other high Cr steels [14,31,33]. Therefore, the present steel exhibits unusual creep behavior, which is characterized by a quite rapid transient creep followed by a pronounced steady-state creep, and, then, tertiary creep stage with a highly accelerated creep rate.

3.2. Microstructural evolution

TMLS with an average PAG size of 26 μm, an average lath thickness of 300 nm and an average dislocation density of 2.6×10^{14} m^{-2} evolved after tempering (Figs. 2 and 3). The {100} pole figure suggests

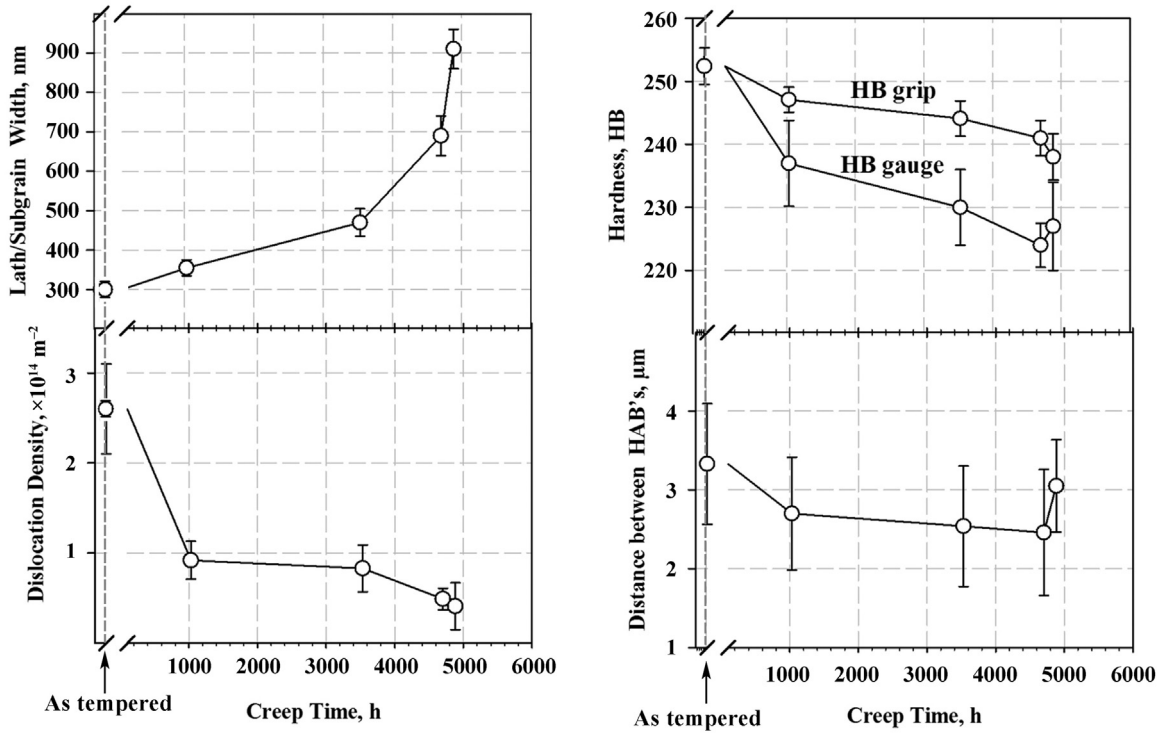

Fig. 4. Changes in the lath/subgrain width, the dislocation density, the hardness, and the distance between HAB in the modified P92 steel during creep at 923 K.

Table 2
The structural parameters of modified P92 steel after tempering and after creep at 923 K under 118 MPa.

Creep time	Tempered	1031 h (0.6%)	3532 h (1.0%)	4701 h (1.5%)	4883 h (ruptured)	Aging at 923 K for 4883 h
Lath/subgrain width, nm	300 ± 20	355 ± 20	470 ± 35	690 ± 50	910 ± 50	440 ± 35
Dislocation density, × 10^{14} m^{-2}	2.60 ± 0.50	0.92 ± 0.21	0.83 ± 0.26	0.49 ± 0.12	0.41 ± 0.26	1.20 ± 0.20
Distance between HABs, μm	3.3 ± 0.8	2.7 ± 0.7	2.5 ± 0.8	2.5 ± 0.8	3.0 ± 0.6	2.9 ± 0.8
Average size of $M_{23}C_6$, nm	66 ± 3	79 ± 3	91 ± 4	101 ± 5	114 ± 8	93 ± 4
Average size of MX, nm	35 ± 5	36 ± 4	39 ± 4	38 ± 5	40 ± 5	38 ± 4
Average size of Laves, nm	–	174 ± 19	292 ± 14	313 ± 20	367 ± 15	305 ± 28

that the martensitic transformation follows Kurdjumov–Sachs orientation relationship [6,34]. The well-defined "Bain circles" [6,35] remain up to tertiary creep, when remarkable spread of "Bain circles" on the {100} pole figures occurs. Moreover, the portions of high-angle boundaries (HAB) with misorientations ranging from 49° to 60° representing the major part of misorientations between the martensite variants are essentially the same in the present steel after tempering and rupture that is an evidence for retaining martensite blocks during creep. Average distances between high-angle boundaries (HABs) of PAGs, packets and blocks remain nearly the same (Figs. 2 and 4, Table 2). On the other hand, the creep leads to the rearrangement of low-angle lath boundaries that leads to insignificant reorientation of crystal lattice within blocks. Therefore, the change in the lath structure is the main process of microstructural evolution during creep.

The transient creep is accompanied by an increase in lath thickness from 300 nm to 350 nm (Figs. 3c, 4, Table 2). The fraction of lath boundaries with misorientations ranging from 2° to 3° decreases, while that for misorientations above 6° increases. It is worth noting that fractions of low-angle boundaries (LAB) with misorientations of 10–15° increases remarkably. Coarsening of lath structure is accompanied by a decrease in the dislocation density by a factor of 2.8 (Table 2), although the frequent band contours on TEM micrographs (Fig. 3c) are indicative of retaining internal elastic stresses. Thus, the mobile lattice dislocations are trapped by low-angle lath boundaries [7,8] that may lead to increasing their misorientations.

The coarsening of lath structure is the main process of microstructural evolution during steady-state creep, while the dislocation density does not change remarkably (Fig. 4, Table 2). At the end of steady-state creep, some laths transform to a structural element with lenticular plate morphology, when the lath grows up to the corresponding block (Fig. 3e). Under tertiary creep the lath structure is replaced by lenticular like plates, which are subdivided into almost equiaxed subgrains with an average size of 910 nm and low angle misorientations. This change in the lath structure during the tertiary creep is accompanied by a twofold decrease in the dislocation density down to 0.4×10^{14} m^{-2} in the ruptured specimen. It is worth noting that TMLS in the grip section of the same ruptured specimen is characterized by a lath thickness of 440 nm and a dislocation density of 1.2×10^{14} m^{-2} (Fig. 3b, Table 2).

3.3. Dispersed particles

The secondary phase particles evolved by tempering have been detailed in previous work [27] and are summarized in Table 2. The

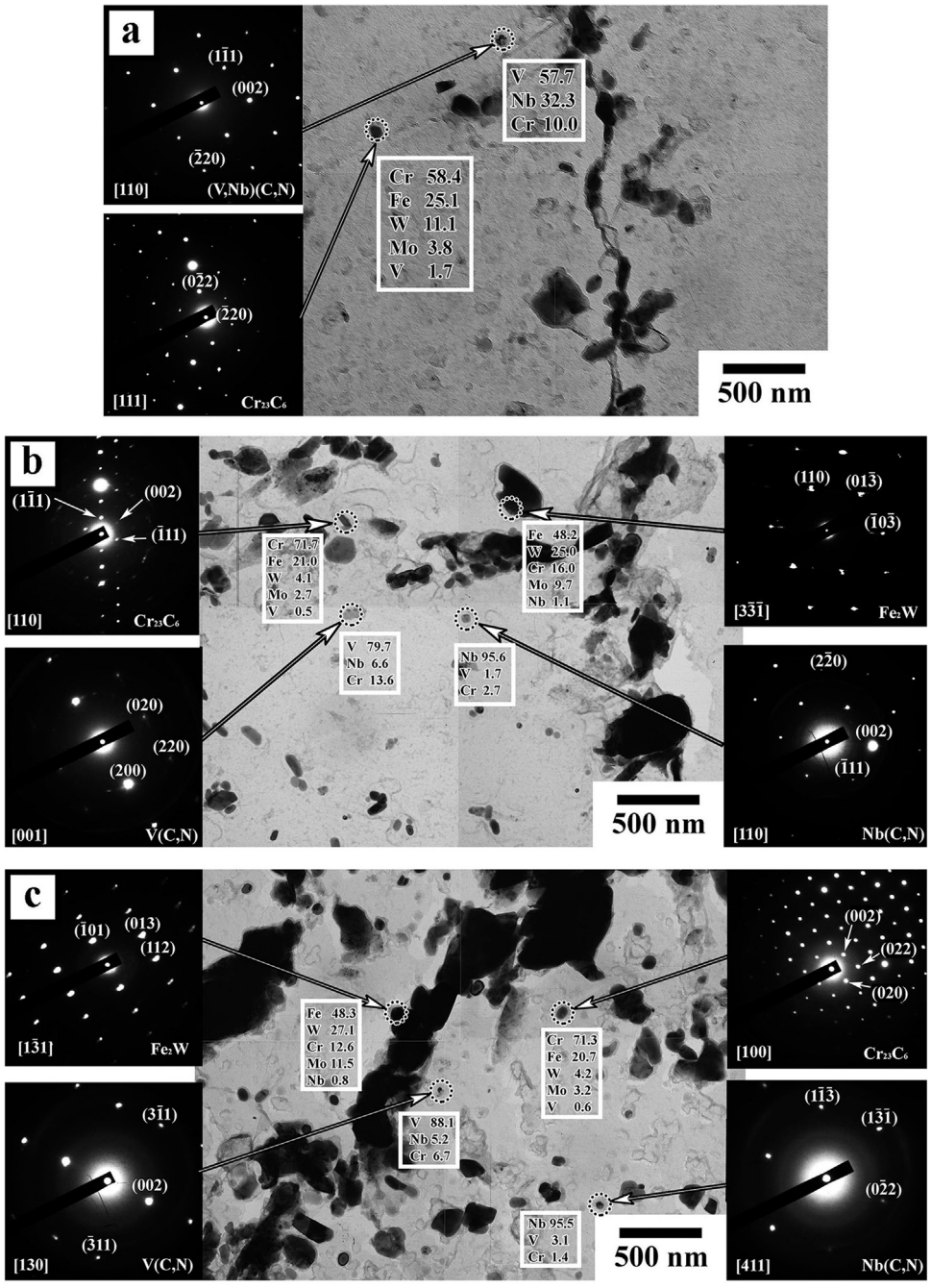

Fig. 5. TEM images of dispersed particles that evolved in the modified P92 steel after tempering (a) and after creep tests for 3532 h (b) and 4883 h (c). The chemical compositions of indicated particles are shown in at.%.

Fig. 5. TEM images of dispersed particles that evolved in the modified P92 steel after tempering (a) and after creep tests for 3532 h (b) and 4883 h (c). The chemical compositions of indicated particles are shown in at%.

$M_{23}C_6$–type carbides frequently precipitate at boundaries of blocks, packets and PAGs (Figs. 3a and 6a). In contrast, these carbides are rarely observed at lath boundaries. Therefore, the boundaries of PAGs, packets and blocks can be considered as preferential sites for precipitation of $M_{23}C_6$-type carbides. The chains of these carbides are clearly seen along various high-angle boundaries. Note here, that the size of $M_{23}C_6$-type carbides located at PAG boundaries is somewhat larger than that located at boundaries of packets and blocks. These carbides exhibit nearly equiaxed shape and contain low amount of tungsten (Fig. 5a); their mean size is 66 nm. Besides $M_{23}C_6$-type carbides, TMLS contains a number of homogeneously distributed (V,Nb)(C,N) carbonitrides. The (V,Nb)(C,N) particles appear with the same morphology and dimensions in the present steel in contrast to those in 9%Cr steel containing 0.05%N, where the shape and size of (V,Nb)(C,N) particles depended on their chemical content, i.e., an enrichment in either Nb or V or Ti [1,4,11–13,21]. In the present steel these

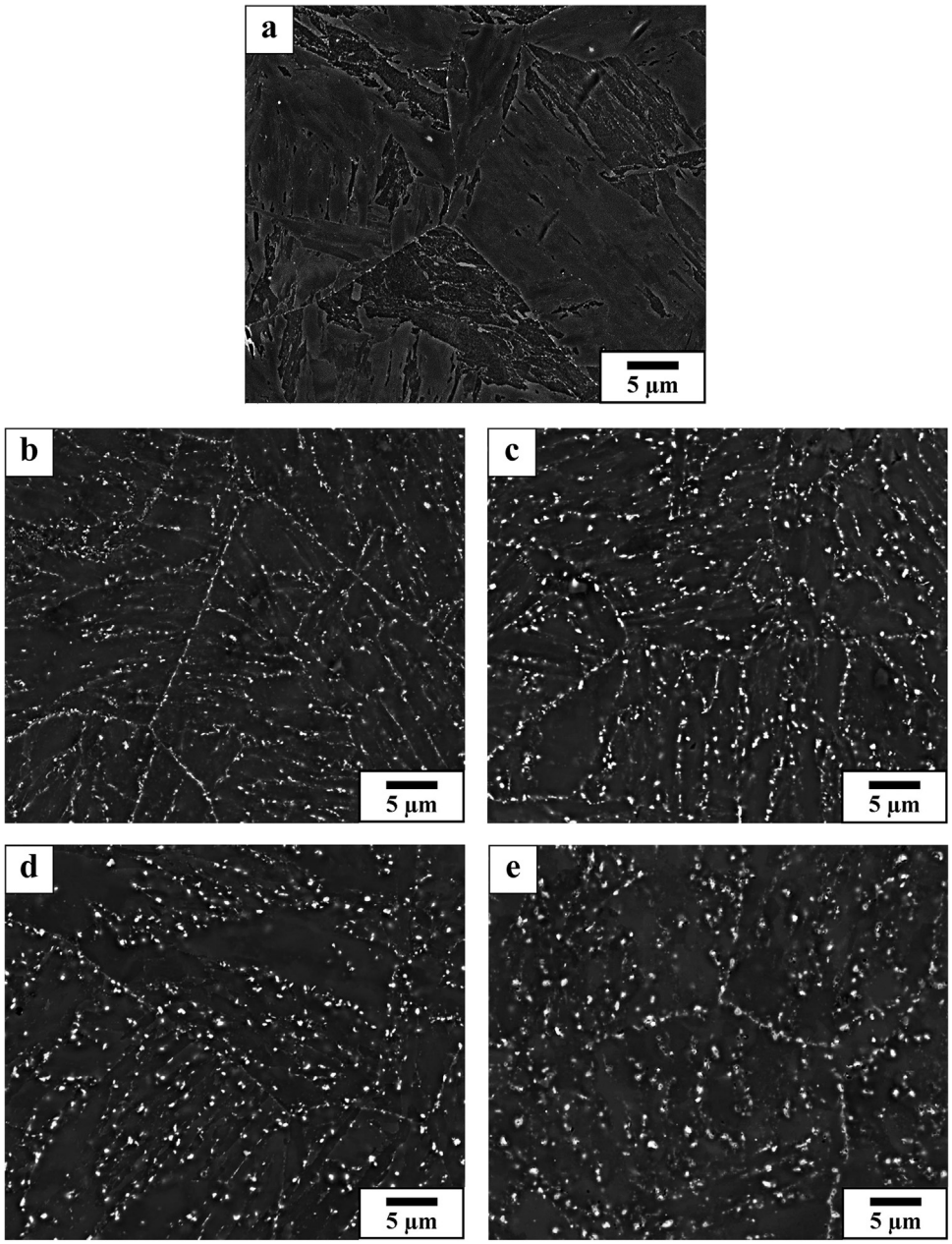

Fig. 6. SEM HAADF micrographs showing Laves phase particles in the modified P92 steel after tempering (a) and creep for 1031 h (b); 3532 h (c); 4701 h (d); and 4883 h (e).

dispersoids exhibit equiaxed shape and an average dimension of 35 nm (Fig. 5a, Table 2).

An aging for sufficiently long time leads to precipitation of Laves phase at boundaries of PAGs, packets, blocks and laths (Fig. 3b) much similar to other high Cr steels [1,3,4,9,11–14,36–42]. The long-time aging for 4883 h is accompanied by significant coarsening of Laves phase particles and $M_{23}C_6$-type carbides to 305 nm and 93 nm, respectively (Table 2). On the other hand, the (V,Nb)(C,N) coarsening occurs with a quite low kinetics. Their size after 4883 h aging increases to 38 nm.

Transient creep leads to precipitation of Laves phase at boundaries of all structural elements in TMLS and insignificant coarsening of $M_{23}C_6$-type carbides (Table 2). Almost continuous chains of Laves phase and $M_{23}C_6$-type carbides appear at boundaries of PAGs and at some portions of packet and block boundaries (Fig. 6). The strain-induced coarsening of Laves phase particles is observed under steady-state and tertiary creep regimes (Table 2). Features of $M_{23}C_6$-type carbides and Laves phase are low content of Σ(Mo + W) and a high W/Mo ratio of about 2.5, respectively, (Fig. 5b and c) that are typical of 3%Co modified P92 steel [12].

The size of (V,Nb)(C,N) carbonitrides increases slightly with increasing the creep strain (Table 2). In contrast to other studies on creep behavior of high-Cr steels [19,20], the development of Z-phase or enrichment of (V,Nb)(C,N) carbonitrides by Cr are not observed in the present study. Two-phase separation between Nb-rich and V-rich carbonitrides becomes more pronounced with increasing creep time

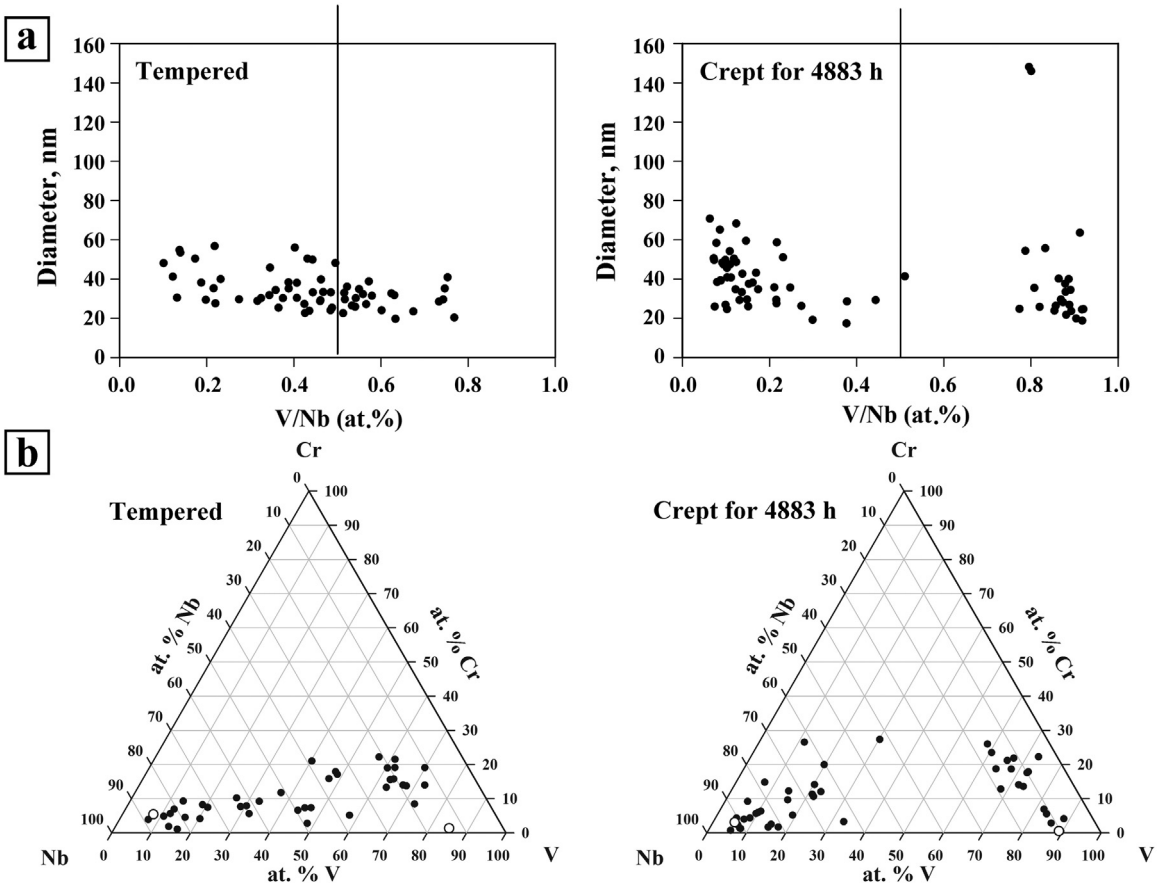

Fig. 7. The size distribution (a) and chemical composition (b) of (Nb,V)(C,N) carbonitrides after tempering and creep for 4883 h in the modified P92 steel. Open circles in (b) represent the calculated equilibrium compositions of Nb(C,N) and V(C,N).

(Figs. 5c and 7), although morphology and dimensions of these two types of (V,Nb)(C,N) dispersoids remain the same. It is clearly seen that a Nb/V ratio in the (V,Nb)(C,N) carbonitride particles examined after tempering spread continuously between the predicted contents (the latter ones are indicated by open circles in Fig. 7b). In contrast, two clearly separated groups with different Nb/V ratios appear at Nb-V-Cr concentration triangle after 4883 h of creep (Fig. 7). Therefore, the (Nb,V)(C,N) carbonitrides nucleate during tempering irrespective of a local Nb/V ratio. Then, these particles tend to exchange their Nb and V content towards more equilibrium concentrations during long term creep.

The Laves phase particles exhibit the fastest coarsening kinetics with a growth exponent of about 2 (Fig. 8). Such a small growth exponent can be associated with particle growth assisted by continuous depletion of solid solution with tungsten and molybdenum in addition to conventional Ostwald ripening [37]. The coarsening behavior of $M_{23}C_6$-type carbides is characterized by a growth exponent of about 9 during long-term ageing and of about 5 during creep (Fig. 8). It should be noted that the rapid coarsening of these carbides at the end of steady-state creep and during accelerated creep was observed (Fig. 8b). This acceleration of particle growth can be associated with a change of their interphase boundary characters. Namely, a gradual loss of orientation relationship between $M_{23}C_6$-type carbides and ferrite matrix with increasing the creep strain can accelerate the coarsening [14,23,33,43].

The particle densities and volume fractions are listed in Table 3. The measured volume fractions of $M_{23}C_6$-type carbides and V-rich carbonitrides in the as-tempered sample are about two times lower than equilibrium ones while the measured and equilibrium volume fractions of Nb-rich carbonitrides are almost the same. On the other hand, the obtained volume fractions of precipitates after creep exposure are in good agreement with those predicted by ThermoCalc. These changes can result from a gradual increase in the volume fraction of $M_{23}C_6$-type carbides towards thermodynamic equilibrium, and a redistribution of alloying elements between the V- and Nb-rich carbonitrides.

The chemical compositions for the $M_{23}C_6$-type carbide and Laves particles obtained by the EDS measurements on carbon extraction replica are shown in Fig. 9 along with equilibrium content calculated by ThermoCalc. The equilibrium content depends on temperature (Table 4). The calculations predict an increase in Cr and Mo and a decrease in Fe and W in $M_{23}C_6$-type carbide under creep since the creep temperature is 100 K lower than the tempering temperature. It is seen that the Cr content approaches thermodynamically equilibrium value during creep, while the increased content of Fe remains. There are two important features of chemical composition of $M_{23}C_6$-type carbides. First, the Mo content is more than twice lower than equilibrium value irrespective of creep strain. Second, these carbides precipitate under tempering with a high V content of 1.6 at%. Such high none-equilibrium content of V in $M_{23}C_6$–type carbides has been sometimes observed and attributed to transformation of V-rich (V,Nb)(C,N) carbonitrides into Z-phase leading to an increase of V in solid solution during long-term aging of 11%Cr steels with $\geq$ 0.05 wt%N [19,20,44,45].

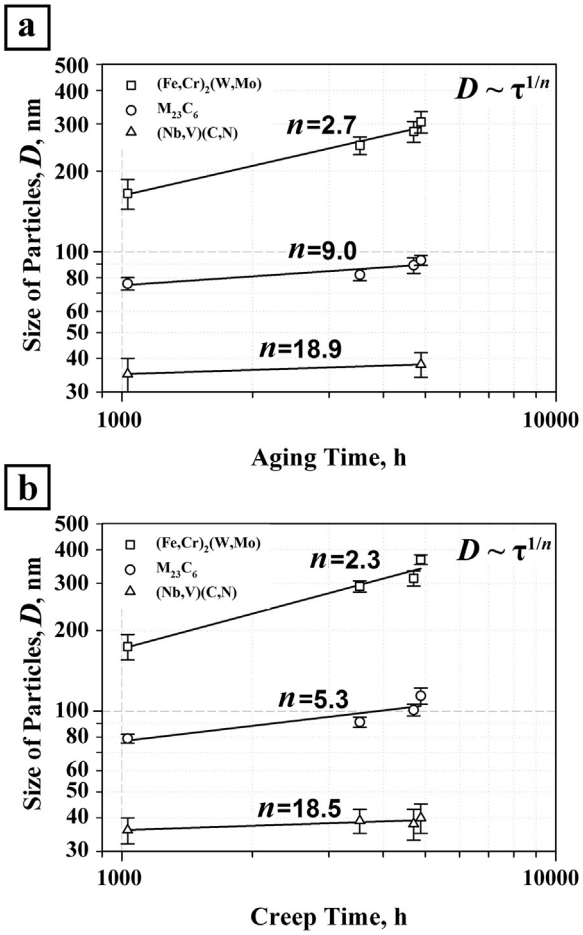

Fig. 8. Evolution of the particle size in the modified P92 steel during long-range aging (a) and creep at 923 K (b).

However, the present steel contains low N content and V depletes from solid solution in the form of $M_{23}C_6$–type carbides, mainly, under tempering. Therefore, a decrease in the V concentrations in $M_{23}C_6$–type carbides may lead to additional precipitation of V-rich (V,Nb)C carbides during creep.

On the other hand, changes of the chemical content of Laves phase are insignificant during creep, since these particles precipitate at a creep temperature. Concentrations of Mo and Nb in Laves phase particles are about twice higher than equilibrium concentrations predicted by ThermoCalc (Fig. 9, Table 3). It is known [40,41] that segregations of Mo at boundaries of TMLS promote the nucleation of Laves phase particles. As a result, a depletion of Mo from ferrite [12,14] occurs in the form of Laves phase. It is obvious that Mo segregates at lath boundaries leading to the precipitation of Laves phase particles at these boundaries. On the other hand, the formation and growth of Laves phase particles are promoted at HABs close to $M_{23}C_6$-type carbides [40]. Therefore, the growth of Laves phase particles located at HABs eventually is accompanied by dissolution of relatively small Laves phase particles located at lath boundaries in accordance with Gibbs-Thomson relationship [46]. It is worth noting that the Laves phases in the present steel are not enriched with Si in contrast to other studies on high-Cr steels with almost the same Si content [40,41]. Perhaps, this is a feature of high B and low N steels providing dense precipitation of Laves phase at lath boundaries during transient creep.

The (V,Nb)(C,N) carbonitride particles are the most stable ones against coarsening. The high value of the growth exponent for these particles is about 19 for long-term aging and creep (Fig. 8). Hence, the mean size of (V,Nb)(C,N) carbonitride particles of 35 ± 5 after tempering does not change significantly during creep (Fig. 7a, Table 2). Only a small amount of particles of V-rich carbonitride with size above 100 nm was observed after creep. The lowered N content in the present steel suppressed the transformation of (V,Nb)(C,N) carbonitrides into Z-phase. The overall volume fraction of (V,Nb)(C,N) carbonitrides remains nearly the same (Table 3). Therefore, the evolution of (V,Nb)(C,N) particles in the present steel is associated with a gradual redistribution of their chemical compositions (Fig. 7b).

3.4. Creep/aging softening

The present steel exhibits relatively high hardness of 252 HB after tempering. Three stages of hardness decrease with different softening rates can be recognized in Fig. 4 for both aging and creep. The first stage of rapid softening is attributed to annihilation of lattice dislocations through the knitting reaction with intrinsic dislocations of lath boundaries having opposite signs [8]. Lath boundaries play a role of sinks for lattice dislocations [8]. The second stage of sluggish hardness decrease is associated with a gradual degradation of TMLS, i.e., lath/particle coarsening, during the steady-state creep. The final third stage correspond to somewhat accelerated softening under tertiary creep that is accompanied by relatively fast kinetics of lath growth, particle coarsening as well as a decrease in the dislocation density. Upon steady-state and tertiary creep the hardness continuously decreases to a value of about 220 HB. In contrast, the formation of subgrain structure during creep in the 3 wt% Co modified P92-type steel has been reported leading to a hardness drop down to 190 HB [12,16,45–47]. Therefore, the transformation of TMLS to subgrain structure is not critically important for the softening of the present steel.

The microstructure evolution during long-term aging and creep of high Cr steels can be described by the following parameter [48]:

$$x = 1 - H_t/H_0 \quad (2)$$

where, H_0 is the hardness in tempered condition, H_t is the hardness after certain aging time or creep strain. It is clearly seen in Fig. 10 that the present steel can withstand creep deformation without significant softening as compared to other P92 + 3%Co steel [49,50].

Table 3
The particle densities and volume fractions.

	Number of particles per unit area (m^{-2})			Volume fractions of precipitates		
	$M_{23}(C,B)_6$	Nb-rich MX	V-rich MX	$M_{23}(C,B)_6$	Nb-rich MX	V-rich MX
Tempered at 1023 K	5.15×10^{12}	7.92×10^{11}	3.07×10^{11}	0.0117	0.000537	0.000144
Crept for 4883 h	3.08×10^{12}	3.73×10^{11}	3.59×10^{11}	0.0210	0.000328	0.000300
ThermoCalc (923 K)	–	–	–	0.0216	0.000476	0.000386

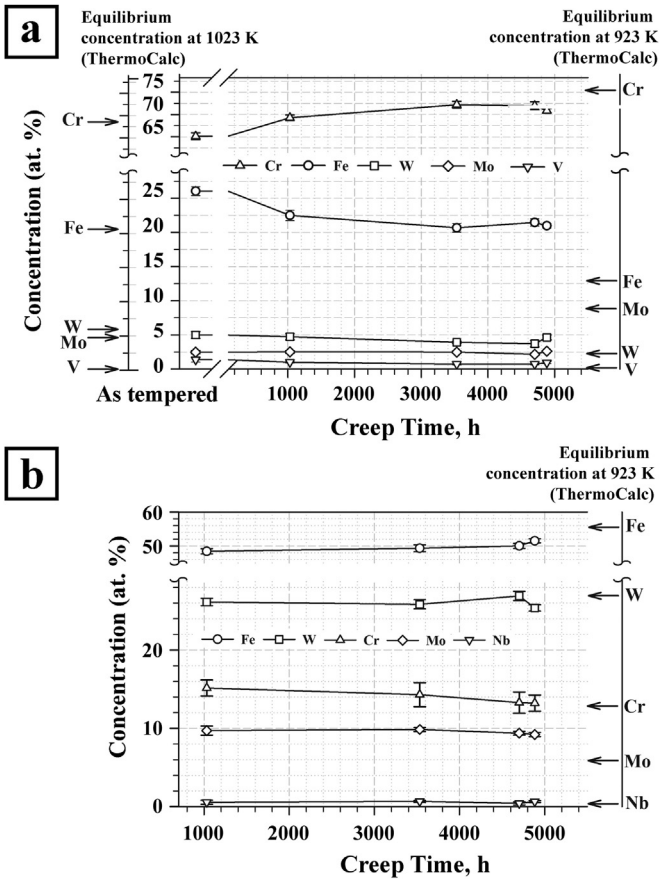

Fig. 9. Chemical composition of $M_{23}C_6$ carbide particles (a) and Laves phase particles (b) as function of creep time in the modified P92 steel.

Table 4
Equilibrium chemical compositions of particles in the modified P92 steel as calculated by ThermoCalc.

Chemical composition, at%		Temperature, K			
		923		1023	
(Nb,V)(C,N)	Nb	91.40	10.43	86.70	13.75
	V	5.51	89.04	7.86	84.90
	Cr	3.08	0.53	5.44	1.35
$(Fe,Cr)_2(W,Mo)$	W	27.86		27.92	
	Fe	55.63		57.05	
	Cr	11.06		9.64	
	Mo	5.11		5.14	
	Nb	0.34		0.25	
$M_{23}C_6$	Cr	75.64		68.20	
	Fe	13.01		21.33	
	Mo	9.01		5.10	
	W	2.33		5.36	
	V	< 0.01		< 0.01	

3.5. Fractography

The fracture surface of the specimen crept for 4883 h is shown in Fig. 11. The dimple rupture occurred in a transgranular fracture path. The large dimples usually are nucleated by particles located on the bottom of these dimples and grow to a very large size before coalescence [51]. Commonly, creep is accompanied by nucleation of voids on boundary particles reducing ductility. Numerous fine dimples are seen in Fig. 11 at ridges between coarse dimples. Therefore, the coarse second phase particles located at boundaries serve as microvoid-nucleating sites leading to the formation of coarse dimples; and the rupture occurs after considerable plastic deformation of ferrite matrix. Thus, the fracture mechanism of the present steel is typical of high Cr steels [12,52].

4. Discussion

4.1. Evolution of TMLS

TMLS in the present steel is characterized by improved stability against coarsening during creep as compared with P92-type steels with or without 3 wt%Co additions [4,11,12] (Fig. 12a). The rate of lath/subgrain growth progressively increases during steady-state and tertiary creep regimes. Increased B and decreased N contents retard the transformation of lath boundaries to subgrain boundaries followed by subgrain coarsening. The main difference between the present steel and 3 wt% Co modified P92-type steels is smaller strains for the onset of steady-state and tertiary creep regimes. The variation in the lath/subgrain growth rate is frequently considered as a function of creep strain [18,53]. The lath/subgrain coarsening behavior of high-Cr steels can be expressed by the following empirical equation [8,18,53–55]:

$$\lg d = \lg d_{ss} + \lg(d_0/d_{ss})\cdot\exp(-\varepsilon/0.12) \quad (3)$$

where d_{SS} is the lath thickness or subgrain dimension at a creep strain of ε, d_0 is the lath thickness in tempered condition. It is seen in Fig. 12b that Eq. (3) well describes the coarsening of crystallites delimitated by LABs in all P92-type steels. It is worth noting that the lath/subgrain sizes obtained in the present study coincide well with others studies [4,11,12], when plotted versus creep strain (Fig. 12b), although the creep times are quite different (Fig. 12a). Therefore, modification of chemical composition of the present steel has a week effect on the strain dependence of microstructural evolution. In contrast to other P92-type steels, however, the lath/subgrain growth in the present steel during creep is not accompanied by significant softening [1,12,15,16,18].

There is a difference between microstructural evolution in the present steel and a 10%Cr with high B and low N contents, which exhibited a rupture time of 39 437 h at an applied stress of 120 MPa [14,30]. TMLS retains in the 10%Cr steel up to rupture. In the present steel the evolution of TMLS to subgrain structure occurs as follows (Fig. 13). A gradual lath coarsening takes place during the steady-state creep. Then, a lenticular plate morphology develops owing to replacement of thin laths by large plates at the end of steady-state creep, leading to tertiary creep. Next, the subgrain structure develops just before rupture. It is obvious that the onset of tertiary creep with a highly accelerated creep rate is attributed to the transformation of lath-type substructure to lenticular-type one followed by the formation of coarse subgrains.

4.2. Particle coarsening and creep behavior

The Laves phase precipitations at lath boundaries (Fig. 13) supports stability of TMLS and a rapid decrease in the creep rate during the transient creep, which is characterized by a high $d\ \ln\varepsilon/d\varepsilon$ value. The transient creep in high-Cr steels is attributed to a decrease in the high dislocation density resulted from martensitic transformation towards the steady-state dislocation substructure [1,56]. The creep rate during transient creep can be expressed by the empirical Andrade creep law predicting a decrease in the strain rate with time t according to [1]:

$$\dot{\varepsilon} \propto t^{-2/3} \quad (4)$$

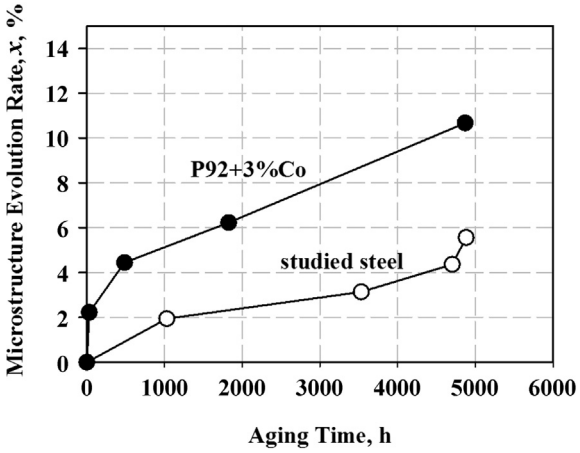

Fig. 10. The change in microstructure related parameter, x, derived from hardness with aging time for P92 + 3%Co [12] and the studied steel.

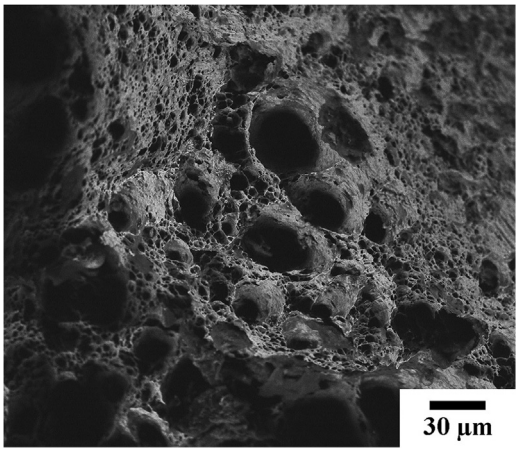

Fig. 11. SEM image of the fractured surface after creep for 4883 h at 923 K.

It is clear that Eq. (4) provides large underestimation of creep rate for the present steel. Abe [37] suggested that the fine precipitation of Laves phase may result in a strong decrease in the creep rate during the transient creep. The Laves phase particles precipitated at lath boundaries during transient creep creates strong obstacles for the dislocation glide along the laths as schematically shown in Fig. 14. These particles play a role of effective pinning agents in addition to (V,Nb)(C,N) carbonitrides and lath boundaries [7,8,10].

The TMLS stability under creep conditions depends mainly on the coarsening behavior of dispersed particles [1–4,8–14,18]. The growth of various dispersed particles in the present steel during creep is represented in Fig. 15 with reference to other studies on similar P92-type steels subjected to creep under the same conditions [4,11]. The size of Laves phase particles in the present steel is smaller than that in a standard P92 steel, but almost the same as that in other P92-type steel modified by 3%Co irrespective of creep duration. The (V,Nb)(C,N) carbonitrides are the smallest dispersed particles in high-Cr steels. The size of finely dispersed (V,Nb)(C,N) carbonitrides in the present steel does not differ remarkably from that in other P92-type steels. The coarsening behavior of (V,Nb)(C,N) particles in the present steel is characterized by almost the same creep time dependence as observed in other steels (Fig. 15), although the creep durations were different.

In contrast, the $M_{23}C_6$-type carbide particles in the present steel are

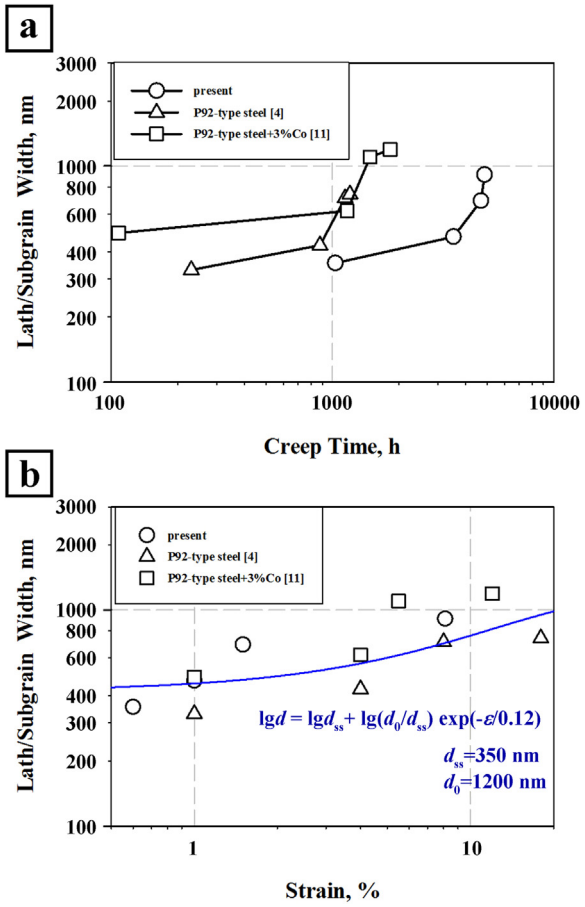

Fig. 12. The subgrain width versus creep time (a) and strain (b) in P92-type steels.

significantly finer than those in other steels including 3%Co modified one at all the studied creep times. It should be noted that the present steel is characterized by smaller (approx. two times) size of $M_{23}C_6$ carbide particles just after tempering as compared to others with normal boron content. The interactions of boron with misfit boundary dislocations may reduce the inter-phase boundary energy and, therefore, decrease the critical size of carbide nuclei. According to $r_0 = 2\sigma/\Delta g_u$ [57], where Δg_u is the difference in molar Gibbs energy between $M_{23}C_6$ carbides and ferrite matrix, the critical radius of nuclei (r_0), is linearly dependent on the interfacial energy (σ). The Gibbs energy of the formation of $M_{23}C_6$-type carbides at 650 °C in the present steel as calculated by ThermoCalc is slightly lower ($-$ 47.4 kJ mol^{-1} for $M_{23}C_6$ and $-$ 47.7 kJ mol^{-1} for $M_{23}(B,C)_6$) than that in a standard P92 steel ($-$ 46.1 kJ mol^{-1} for $M_{23}C_6$). Such difference in the Gibbs energy suggests the change of the nucleus size of 1.03. Thus, the difference in the particle size in the present steel and other P92-type ones after tempering can be associated with the change in interfacial energy. Assuming that the average particle size in these steels after tempering is close to the critical one, it may be concluded that the value of the interfacial energy in the studied steel is about 0.6–0.7 of that in standard P92 and P92 + 3%Co steels [4,11]. It should also be noted that the lowered value of the interfacial energy for these carbides with a ferrite matrix in the present steel should retard the coarsening of carbide particles during creep. Therefore, these relatively fine carbide particles remain at nanometer scale (below 100 nm) until the accelerated creep stage. Aforementioned two-phase separation of $M_{23}C_6$-type carbides in

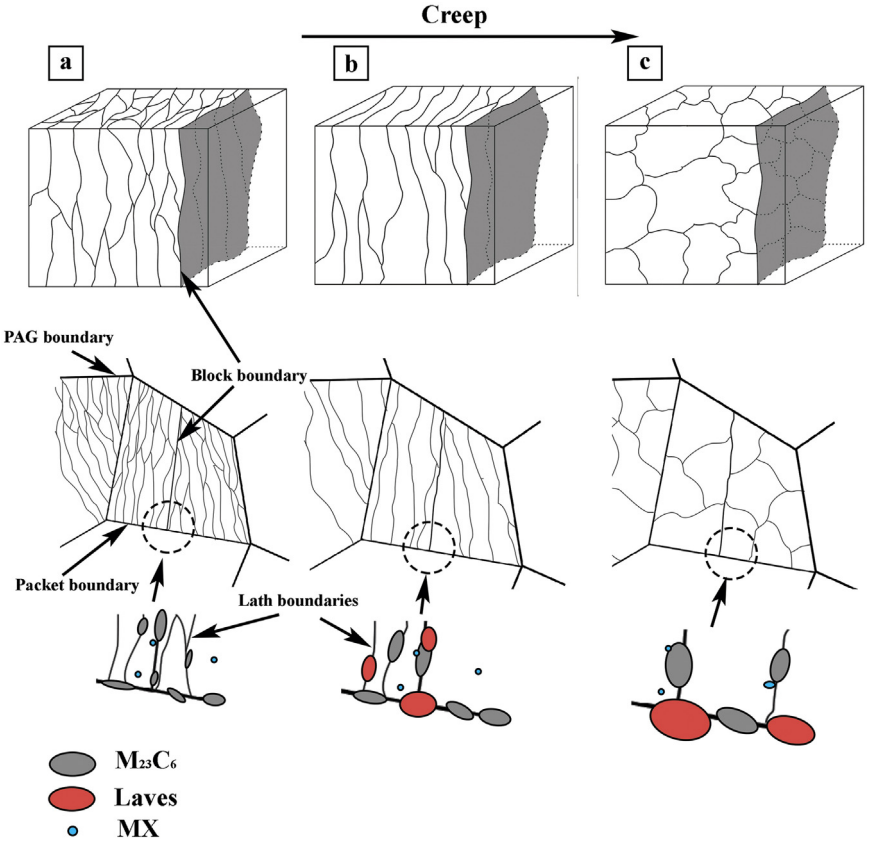

Fig. 13. Schematic illustration of the microstructural evolution during creep: TMLS evolved after tempering(a); the formation of crystallites delimitated by LABs and having plate-like shape at the onset of tertiary creep (b); the formation of subgrain structure during tertiary creep (c).

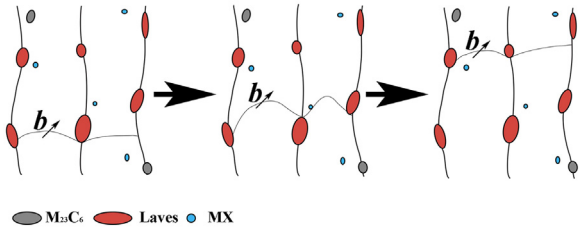

Fig. 14. Schematic presentation of dislocation glides at steady-state creep.

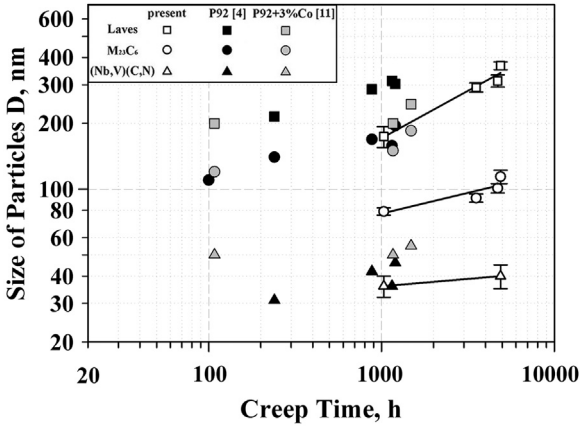

Fig. 15. Particle growth kinetic in P92-type steels.

the present steel can also decrease the coarsening rate in comparison with other P92-type steels (Fig. 15).

The volume fraction of $M_{23}C_6$-type particles is significantly larger than that of other dispersed particles, i.e., Laves phase and (V,Nb)(C,N) carbonitrides (Table 3). Numerous $M_{23}C_6$-type particles were considered as the main contributors to the stability of the tempered martensite lath structure during creep at elevated temperatures [2,9,54]. A decrease in the carbide particles size by a factor of approx. 1.5 as compared to other P92-type steels results in corresponding increase in both the Zener pining pressure and the Orowan strengthening in the present steel. Therefore, the enhanced stability of tempered martensite lath structure in the present steel can result from the refinement of $M_{23}C_6$-type carbides upon tempering and the stabilization of $M_{23}C_6$-type particles against coarsening during creep.

5. Conclusions

The changes in the tempered martensite lath structure and the dispersed particles were studied in a 3%Co modified P92-type steel with lowered nitrogen content and increased boron content subjected to creep at 923 K under 120 MPa. The main results can be summarized as follows.

1. The dislocation density in the lath/subgrain interiors decreased from 2.6×10^{-14} m^{-2} (just after tempering) to 0.4×10^{-14} m^{-2} during creep for 4883 h (creep failure), while the transverse size of lath/subgrains increased from 300 nm to 910 nm. The dislocation density rapidly decreased by a factor of 2.5 during the transient creep followed by a sluggish decrease upon further creep, whereas the most significant changes in the lath/subgrain size occurred during the accelerated creep stage. The present steel is characterized by a low creep/aging softening as compared to other P92-type steels that can be associated with a relatively low coarsening rate of precipitates and delayed subgrain transformation.
2. The dispersed precipitates consisted of various secondary phases

including $M_{23}C_6$-type carbides and (Nb,V)(C,N)-type carbonitrides, both of which precipitated during tempering, and Laves phase precipitated during creep. The particles exhibited different coarsening behavior during creep. The particle growth exponents were approx. 2, 5 and 19 for Laves phase, $M_{23}C_6$ carbides and (Nb,V)(C,N) carbonitrides, respectively. Coarsening of the $M_{23}C_6$ carbides during creep was accompanied by a gradual increase in their volume fraction approaching thermodynamic equilibrium.

3. The chemical composition of Laves phase was close to equilibrium and did not vary remarkably during creep, while that of $M_{23}C_6$ carbides somewhat changed in accordance with temperature dependence of equilibrium composition because of difference in the nucleation temperature (tempering at 1023 K) and the creep temperature (923 K). In contrast, the (Nb,V)(C,N) carbonitrides appeared during tempering as non-equilibrium precipitates, which were characterized by a wide range of Nb/V ratios. The chemical composition of (Nb,V)(C,N) particles was gradually changed during creep leading to the development of enriched with either Nb or V carbonitrides as predicted by ThermoCalc calculations.
4. The present steel exhibited superior creep resistance as compared to other P92-type steels crept under the same conditions that could be associated with improved stability of tempered martensite lath structure and dispersed particles. Both the laths/subgrains and the dispersed particles in the present steel could be qualitatively characterized by ordinary coarsening behaviors during creep similar to other P92-type steels. However, the sizes of laths/subgrains and dispersed particles in the present steel were remarkably smaller than those in other steels of similar types.
5. The high creep rate at tertiary stage could be associated with the transformation of the lath structure to lenticular-type one followed by the formation of well-defined coarse subgrains. This sequence of structural changes was assisted by a strain-induced coarsening of Laves phase particles and $M_{23}C_6$-type carbide particles located at various boundaries during steady-state and tertiary creep stages.

Acknowledgement

The study was financial supported by the Ministry of Education and Science of Russian Federation, under project of Government Task No. 11.2868.2017/PCh. The authors are grateful to the staff of the Joint Research Center, "Technology and Materials", Belgorod State University, for providing the equipment for instrumental analysis.

References

[1] Abe, T.U. Kern, R. Viswanathan, Creep-Resist. Steels (2008), http://dx.doi.org/10.1533/9781845694012.
[2] R.O. Kaybyshev, V.N. Skorobogatykh, I. a. Shchenkova, New martensitic steels for fossil power plant: creep resistance, Phys. Met. Metallogr. 109 (2010) 186–200, http://dx.doi.org/10.1134/S0031918X10020110.
[3] P.J. Ennis, A. Zielinska-Lipiec, O. Wachter, A. Czyrska-Filemonowicz, Microstructural stability and creep rupture strength of the martensitic steel P92 for advanced power plant, Acta Mater. 45 (1997) 4901–4907, http://dx.doi.org/10.1016/S1359-6454(97)00176-6.
[4] V. Dudko, A. Belyakov, D. Molodov, R. Kaibyshev, Microstructure evolution and pinning of boundaries by precipitates in a 9 pct Cr heat resistant steel during creep, Metall. Mater. Trans. A Phys. Metall. Mater. Sci. 44 (2013), http://dx.doi.org/10.1007/s11661-011-0899-1.
[5] T. Sakthivel, S.P. Selvi, K. Laha, An assessment of creep deformation and rupture behaviour of 9Cr-1.8W-0.5Mo-VNb (ASME grade 92) steel, Mater. Sci. Eng. A 640 (2015) 61–71, http://dx.doi.org/10.1016/j.msea.2015.05.068.
[6] H. Kitahara, R. Ueji, N. Tsuji, Y. Minamino, Crystallographic features of lath martensite in low-carbon steel, Acta Mater. 54 (2006) 1279–1288, http://dx.doi.org/10.1016/j.actamat.2005.11.001.
[7] M. Mitsuhara, S. Yamasaki, M. Miake, H. Nakashima, M. Nishida, J. Kusumoto, A. Kanaya, Creep strengthening by lath boundaries in 9Cr ferritic heat-resistant steel, Philos. Mag. Lett. 96 (2016) 76–83, http://dx.doi.org/10.1080/09500839.2016.1154200.
[8] V. Dudko, A. Belyakov, R. Kaibyshev, Evolution of Lath Substructure and Internal Stresses in a 9% Cr Steel during Creep, ISIJ Int. 57 (2017) 540–549, http://dx.doi.org/10.2355/isijinternational.ISIJINT-2016-334.
[9] A. Kostka, K.G. Tak, R.J. Hellmig, Y. Estrin, G. Eggeler, On the contribution of carbides and micrograin boundaries to the creep strength of tempered martensite ferritic steels, Acta Mater. 55 (2007) 539–550, http://dx.doi.org/10.1016/j.actamat.2006.08.046.
[10] V. Dudko, A. Belyakov, R. Kaibyshev, Origin of threshold stresses in a P92-type steel, Trans. Indian Inst. Met. 69 (2016) 223–227, http://dx.doi.org/10.1007/s12666-015-0757-8.
[11] N. Dudova, A. Plotnikova, D. Molodov, A. Belyakov, R. Kaibyshev, Structural changes of tempered martensitic 9%Cr-2%W-3%Co steel during creep at 650°C, Mater. Sci. Eng. A 534 (2012) 632–639, http://dx.doi.org/10.1016/j.msea.2011.12.020.
[12] A. Fedoseeva, N. Dudova, R. Kaibyshev, Creep strength breakdown and microstructure evolution in a 3%Co modified P92 steel, Mater. Sci. Eng. A 654 (2016) 1–12, http://dx.doi.org/10.1016/j.msea.2015.12.027.
[13] A. Fedoseeva, N. Dudova, R. Kaibyshev, Creep behavior and microstructure of a 9Cr–3Co–3W martensitic steel, J. Mater. Sci. (2017), http://dx.doi.org/10.1007/s10853-016-0595-z.
[14] R. Mishnev, N. Dudova, A. Fedoseeva, R. Kaibyshev, Microstructural aspects of superior creep resistance of a 10%Cr martensitic steel, Mater. Sci. Eng. A 678 (2016) 178–189, http://dx.doi.org/10.1016/j.msea.2016.09.096.
[15] H.G. Armaki, R. Chen, K. Maruyama, M. Igarashi, Creep behavior and degradation of subgrain structures pinned by nanoscale precipitates in strength-enhanced 5 to 12 Pct Cr ferritic steels, Metall. Mater. Trans. A Phys. Metall. Mater. Sci. 42 (2011) 3084–3094, http://dx.doi.org/10.1007/s11661-011-0726-8.
[16] H. Ghassemi-Armaki, R.P. Chen, K. Maruyama, M. Igarashi, Contribution of recovery mechanisms of microstructure during long-term creep of Gr.91 steels, J. Nucl. Mater. 433 (2013) 23–29, http://dx.doi.org/10.1016/j.jnucmat.2012.09.026.
[17] F. Abe, Creep behavior, deformation mechanisms, and creep life of Mod.9Cr-1Mo Steel, Metall. Mater. Trans. A Phys. Metall. Mater. Sci. 46 (2015) 5610–5625, http://dx.doi.org/10.1007/s11661-015-3144-5.
[18] A. Aghajani, C. Somsen, G. Eggeler, On the effect of long-term creep on the microstructure of a 12% chromium tempered martensite ferritic steel, Acta Mater. 57 (2009) 5093–5106, http://dx.doi.org/10.1016/j.actamat.2009.07.010.
[19] L. Cipolla, H.K. Danielsen, D. Venditti, P.E. Di Nunzio, J. Hald, M.A.J. Somers, Conversion of MX nitrides to Z-phase in a martensitic 12% Cr steel, Acta Mater. 58 (2010) 669–679, http://dx.doi.org/10.1016/j.actamat.2009.09.045.
[20] H.K. Danielsen, Review of Z phase precipitation in 9–12 wt%Cr steels, Mater. Sci. Technol. 32 (2016) 126–137, http://dx.doi.org/10.1179/1743284715Y.0000000066.
[21] Y. Xu, Y. Nie, M. Wang, W. Li, X. Jin, The effect of microstructure evolution on the mechanical properties of martensite ferritic steel during long-term aging, Acta Mater. 131 (2017) 110–122, http://dx.doi.org/10.1016/j.actamat.2017.03.045.
[22] J. Hartford, Interface energy and electron structure for Fe/VN, Phys. Rev. B - Condens. Matter Mater. Phys. 61 (2000) 2221–2229, http://dx.doi.org/10.1103/PhysRevB.61.2221.
[23] A. Fedoseeva, E. Tkachev, V. Dudko, N. Dudova, R. Kaibyshev, Effect of alloying on interfacial energy of precipitation/matrix in high-chromium martensitic steels, J. Mater. Sci. 52 (2017) 4197–4209, http://dx.doi.org/10.1007/s10853-016-0654-5.
[24] R. Sahara, T. Matsunaga, H. Hongo, M. Tabuchi, Theoretical investigation of stabilizing mechanism by boron in body-centered cubic iron through (Fe,Cr)23(C,B)6 precipitates, Metall. Mater. Trans. A Phys. Metall. Mater. Sci. 47 (2016) 2487–2497, http://dx.doi.org/10.1007/s11661-016-3397-7.
[25] N. Dudova, R. Kaibyshev, On the precipitation sequence in a 10%Cr steel under tempering, ISIJ Int. 51 (2011) 826–831, http://dx.doi.org/10.2355/isijinternational.51.826.
[26] H. Semba, F. Abe, Alloy design and creep strength of advanced 9%Cr USC boiler steels containing high concentration of boron, Energy Mater. 1 (2006) 238–244, http://dx.doi.org/10.1179/174892406X173611.
[27] I. Fedorova, A. Kostka, E. Tkachev, A. Belyakov, R. Kaibyshev, Tempering behavior of a low nitrogen boron-added 9%Cr steel, Mater. Sci. Eng. A 662 (2016) 443–455, http://dx.doi.org/10.1016/j.msea.2016.03.092.
[28] M. Tabuchi, H. Hongo, F. Abe, Creep strength of dissimilar welded joints using high B-9Cr steel for advanced USC boiler, Metall. Mater. Trans. A Phys. Metall. Mater. Sci. 45 (2014) 5068–5075, http://dx.doi.org/10.1007/s11661-014-2471-2.
[29] K. Kimura, K. Sawada, H. Kushima, K. Kubo, Effect of stress on the creep deformation of ASME Grade P92/T92 steels, Int. J. Mater. Res. 99 (2008) 395–401, http://dx.doi.org/10.3139/146.101651.
[30] J. Vanaja, K. Laha, M.D. Mathew, Effect of tungsten on primary creep deformation and minimum creep rate of reduced activation ferritic-martensitic steel, Metall. Mater. Trans. A Phys. Metall. Mater. Sci. 45 (2014) 5076–5084, http://dx.doi.org/10.1007/s11661-014-2472-1.
[31] J. Vanaja, K. Laha, Assessment of tungsten content on tertiary creep deformation behavior of reduced activation ferritic–martensitic steel, Metall. Mater. Trans. A Phys. Metall. Mater. Sci. 46 (2015) 4669–4679, http://dx.doi.org/10.1007/s11661-015-3075-1.
[32] F. Garofalo, Fundamentals of Creep and Creep Rupture in Metals, MacMillan, New York, 1965.
[33] R. Kaibyshev, R. Mishnev, E. Tkachev, N. Dudova, Effect of Ni and Mn on the creep behaviour of 9-10 %Cr steels with low N and high B, Trans. Indian Inst. Met. 69 (2016) 203–210, http://dx.doi.org/10.1007/s12666-015-0761-z.
[34] L. Qi, A.G. Khachaturyan, J.W. Morris, The microstructure of dislocated martensitic steel: theory, Acta Mater. 76 (2014) 23–39, http://dx.doi.org/10.1016/j.actamat.2014.04.038.
[35] R. Mishnev, N. Dudova, R. Kaibyshev, Low cycle fatigue behavior of a 10Cr-2W-Mo-3Co-NbV steel, Int. J. Fatigue 83 (2016) 344–355, http://dx.doi.org/10.1016/j.ijfatigue.2015.11.008.
[36] I. Fedorova, A. Belyakov, P. Kozlov, V. Skorobogatykh, I. Shenkova, R. Kaibyshev,

Laves-phase precipitates in a low-carbon 9% Cr martensitic steel during aging and creep at 923K, Mater. Sci. Eng. A 615 (2014) 153–163, http://dx.doi.org/10.1016/j.msea.2014.07.046.
[37] F. Abe, Effect of fine precipitation and subsequent coarsening of Fe2W laves phase on the creep deformation behavior of tempered martensitic 9Cr-W steels, Metall. Mater. Trans. A 36 (2005) 321–332, http://dx.doi.org/10.1007/s11661-005-0305-y.
[38] L. Maddi, G.S. Deshmukh, A.R. Ballal, D.R. Peshwe, R.K. Paretkar, K. Laha, M.D. Mathew, Effect of Laves phase on the creep rupture properties of P92 steel, Mater. Sci. Eng. A 668 (2016) 215–223, http://dx.doi.org/10.1016/j.msea.2016.05.074.
[39] X.Z. Zhang, X.J. Wu, R. Liu, J. Liu, M.X. Yao, Influence of Laves phase on creep strength of modified 9Cr-1Mo steel, Mater. Sci. Eng. A 706 (2017) 279–286, http://dx.doi.org/10.1016/j.msea.2017.08.111.
[40] M.I. Isik, A. Kostka, V.A. Yardley, K.G. Pradeep, M.J. Duarte, P.P. Choi, D. Raabe, G. Eggeler, The nucleation of Mo-rich Laves phase particles adjacent to M23C6 micrograin boundary carbides in 12% Cr tempered martensite ferritic steels, Acta Mater. 90 (2015) 94–104, http://dx.doi.org/10.1016/j.actamat.2015.01.027.
[41] M.I. Isik, A. Kostka, G. Eggeler, On the nucleation of Laves phase particles during high-temperature exposure and creep of tempered martensite ferritic steels, Acta Mater. 81 (2014) 230–240, http://dx.doi.org/10.1016/j.actamat.2014.08.008.
[42] A. Fedoseeva, N. Dudova, U. Glatzel, R. Kaibyshev, Effect of W on tempering behaviour of a 3 %Co modified P92 steel, J. Mater. Sci. 51 (2016) 9424–9439, http://dx.doi.org/10.1007/s10853-016-0188-x.
[43] A. Kipelova, A. Belyakov, R. Kaibyshev, The crystallography of M23C6 carbides in a martensitic 9% Cr steel after tempering, aging and creep, Philos. Mag. 93 (2013) 2259–2268, http://dx.doi.org/10.1080/14786435.2013.765995.
[44] Y. Xu, X. Zhang, Y. Tian, C. Chen, Y. Nan, H. He, M. Wang, Study on the nucleation and growth of M23C6carbides in a 10% Cr martensite ferritic steel after long-term aging, Mater. Charact. 111 (2016) 122–127, http://dx.doi.org/10.1016/j.matchar.2015.11.023.
[45] Z.F. Peng, S. Liu, C. Yang, F.Y. Chen, F.F. Peng, The effect of phase parameter variation on hardness of P91 components after service exposures at 530–550 °C, Acta Mater. 143 (2018) 141–155, http://dx.doi.org/10.1016/j.actamat.2017.10.010.
[46] D.A. Porter, K.E. Esterling, M. Sherif, Phase Transformation in Metals and Alloys, third ed., CRS Press, Boca Raton, FL, 2009.
[47] V. Dudko, A. Belyakov, V. Skorobogatyh, I. Schenkova, R. Kaibyshev, Dynamic polygonization in 9%Cr heat resistant steel, J. Phys. Conf. Ser. (2010), http://dx.doi.org/10.1088/1742-6596/240/1/012070.
[48] H. Wang, W. Yan, S. van Zwaag, Q. Shi, W. Wang, K. Yang, Y. Shan, On the 650 °C thermostability of 9–12Cr heat resistant steels containing different precipitates, Acta Mater. 134 (2017) 143–154, http://dx.doi.org/10.1016/j.actamat.2017.05.069.
[49] A. Fedoseeva, N. Dudova, R. Kaibyshev, Microstructural evolution in a 9%Cr-3%Co-3%W-VNb steel during creep, Mater. Sci. Forum (2017), http://dx.doi.org/10.4028/www.scientific.net/MSF.879.548.
[50] F. Masuyama, Hardness model for creep-life assessment of high-strength martensitic steels, Mater. Sci. Eng. A 510–511 (2009) 154–157, http://dx.doi.org/10.1016/j.msea.2008.04.133.
[51] ASM Handbook, Fractography, Materials Park, OH, ASM, 1987.
[52] T. Shrestha, M. Basirat, I. Charit, G.P. Potirniche, K.K. Rink, Creep rupture behavior of Grade 91 steel, Mater. Sci. Eng. A 565 (2013) 382–391, http://dx.doi.org/10.1016/j.msea.2012.12.031.
[53] R. Agamennone, W. Blum, C. Gupta, J.K. Chakravartty, Evolution of microstructure and deformation resistance in creep of tempered martensitic 9-12%Cr-2%W-5%Co steels, Acta Mater. 54 (2006) 3003–3014, http://dx.doi.org/10.1016/j.actamat.2006.02.038.
[54] K. Maruyama, K. Sawada, J. Koike, Advances in physical metallurgy and processing of steels. strengthening mechanisms of creep resistant tempered martensitic steel, ISIJ Int. 41 (2001) 641–653, http://dx.doi.org/10.2355/isijinternational.41.641.
[55] J. Hald, L. Korcakova, Precipitate stability in creep resistant ferritic steels-experimental investigations and modelling, ISIJ Int. 43 (2003) 420–427, http://dx.doi.org/10.2355/isijinternational.43.420.
[56] W. Blum, P. Eisenlohr, F. Breutinger, Understanding creep—a review, Metall. Mater. Trans. A 33 (2002) 291–303, http://dx.doi.org/10.1007/s11661-002-0090-9.
[57] G. Gottstein, Physical Foundations of Materials Science, Springer, New York, 2004.